

TEXTURED IMAGE SEGMENTATION BASED ON LOCAL SPECTRAL HISTOGRAM AND ACTIVE CONTOUR

Xianghua Xie

Department of Computer Science, University of Wales Swansea, Swansea, U.K.

Keywords: Active contour, Local spectral histogram, Level set method, Texture segmentation, Wasserstein distance.

Abstract: In this paper, we propose a novel level set based active contour model to segment textured images. The proposed method is based on the assumption that local histograms of filtering responses between foreground and background regions are statistically separable. In order to be able to handle texture non-uniformities, which often occur in real world images, we use rotation invariant filtering features and local spectral histograms as image feature to drive the snake segmentation. Automatic histogram bin size selection is carried out so that its underlying distribution can be best represented. Experimental results on both synthetic and real data show promising results and significant improvements compared to direct modeling of filtering responses.

1 INTRODUCTION

Active contours have been increasingly used in analyzing textured images, e.g. (Sandberg et al., 2002; Ni et al., 2007; Houhou and Thiran, 2008; Savelonas et al., 2008). Despite recent advances in edge based approaches, e.g. (Paragios et al., 2004; Xie and Mirmehdi, 2008), region based approaches have some obvious advantages when analyzing heavily texture images in that edge based boundary description can easily be compromised by texture patterns. Region based approach deforms initial contours towards the region/object boundaries of interest by minimizing an energy function, whose minimum ideally collocates with those boundaries. Thus, it is vitally important to use robust features and appropriate region indication/separation functional.

Various features have been investigated in the contour segmentation framework, such as co-occurrence matrices (Pujol and Radeva, 2004), structure tensor (Rousson et al., 2004), and local binary patterns (Savelonas et al., 2008). However, filtering responses are among the most popular approaches, e.g. (Paragios and Deriche, 2002; Sandberg et al., 2002; Aujol et al., 2003; He et al., 2004; Sagiv et al., 2006). In (Sandberg et al., 2002) the authors decompose the image using Gabor filters. The collected filtering responses at each pixel are used to measure the difference between pixels in a piecewise constant model. However, it largely ignores the spatial distribution among local filtering coefficients and this direct com-

parison of filter responses is error prone since the responses can be misaligned due to the anisotropic nature of most of the filters. Wavelet packet transform is used in (Aujol et al., 2003) and the energy distributions in sub-bands are used to characterize textures. One of the main difficulties in dealing with filtering responses is their large dimensionality. It is also challenging to handle textural variations within regions of interest due to, for example, rotation or view point changes, since most of the filters are orientation sensitive.

Once the features are derived, one also needs to decide how to model their distributions so that correct features are included in describing the object of interest. In other words, this modeling provides a region indication or separation functional to drive the active contours. Modeling based on global distribution is a popular approach. For example, in (Paragios and Deriche, 2002; He et al., 2004) Mixture of Gaussians are used to model the image features. Another powerful approach is based on the piecewise constant assumption (Chan and Vese, 2001). It also has been recently adopted in texture segmentation, e.g. (Sandberg et al., 2002; Sagiv et al., 2006; Ni et al., 2007). However, how to cope with texture inhomogeneity is a major challenge.

2 PROPOSED APPROACH

In this paper, we propose a novel region based active contour model, which is based on the assumption that local histograms of filtering responses between object of interest and background regions are statistically separable. Briefly, we first apply a bank of filters to the image, from which we have a set of filter responses at different scales and orientations. These responses are then grouped and condensed so that it can handle textural non-uniformity which may occur in real world images. Reduced, invariant features are thus obtained. This process also effectively decreases the dimensionality of filter feature space, which is beneficial for single image segmentation. We then collect local distributions of these features at each pixels, known as local spectral histograms. These local histograms contains not only directly filtering responses but also their spatial distributions in their local neighborhoods. The optimal bin size for these histograms are obtained by minimizing a mean integrated square error based cost function. An energy minimization problem is thus formulated by fitting two spectral histograms, one of which is used to approximate the foreground region and the other for the background. We will show that this approach is effective to handle texture inhomogeneity, compared to, for example, direct modeling of filtering responses (Sandberg et al., 2002) or local intensity distributions (Ni et al., 2007).

Next, Section 2.1 describes the filter bank and rotation invariant feature selection. Local spectral histogram extraction is presented in Section 2.2 and automatic optimal histogram bin size computation is given in Section 2.3. Finally, Section 2.4 introduces the level set based snake model using these invariant features for image segmentation.

2.1 Filters and Feature Selection

Texture provides important information for recognition and interpolation. Numerous techniques have been reported in the literature to carry out texture analysis. They can be generally categorized in four ways: statistical approaches which measure the spatial distribution of pixel values, structural approaches that are based on analyzing texture primitives and the spatial arrangement of these primitives, filter based approaches which analyze local pixel dependencies using a bank of filters, and model based approaches which often use derived model parameters as texture features. Filter bank based approaches have been popular since they can analyze textures in arbitrary orientations and scales and have been strongly motivated

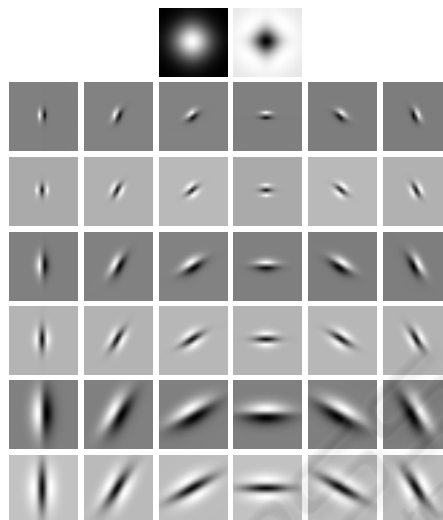


Figure 1: The filter bank consists 38 filters in total, which include one Gaussian filter, one Laplacian of Gaussian filter, and 36 edge and bar filters across 6 orientations and 3 scales.



Figure 2: An example testing image.

by psychological studies of human vision system.

However, filter bank based methods often result in high dimensional feature space which can be difficult to handle for certain applications. Unlike image classification, in snake based image segmentation, we may not have enough features extracted from a single image to populate the high dimensional feature space in order to accurately estimate the underlying feature distributions. Moreover, there are usually significant amount of redundant information among the filtering responses. For example, a set of anisotropic filters will get the same responses from isotropic image regions. Fig. 1 shows a bank of filters which has been used in (Varma and Zisserman, 2002) for image classification. It contains two isotropic filters and thirty six anisotropic filters. The two isotropic filters are Gaussian and Laplacian of Gaussian both with $\sigma = 10$. Those thirty six anisotropic filters come from two families, edges and bars, each of which consists filters at three progressive scales, i.e. $(\sigma_x, \sigma_y) = \{(1,3), (2,6), (4,12)\}$, and six uniformly

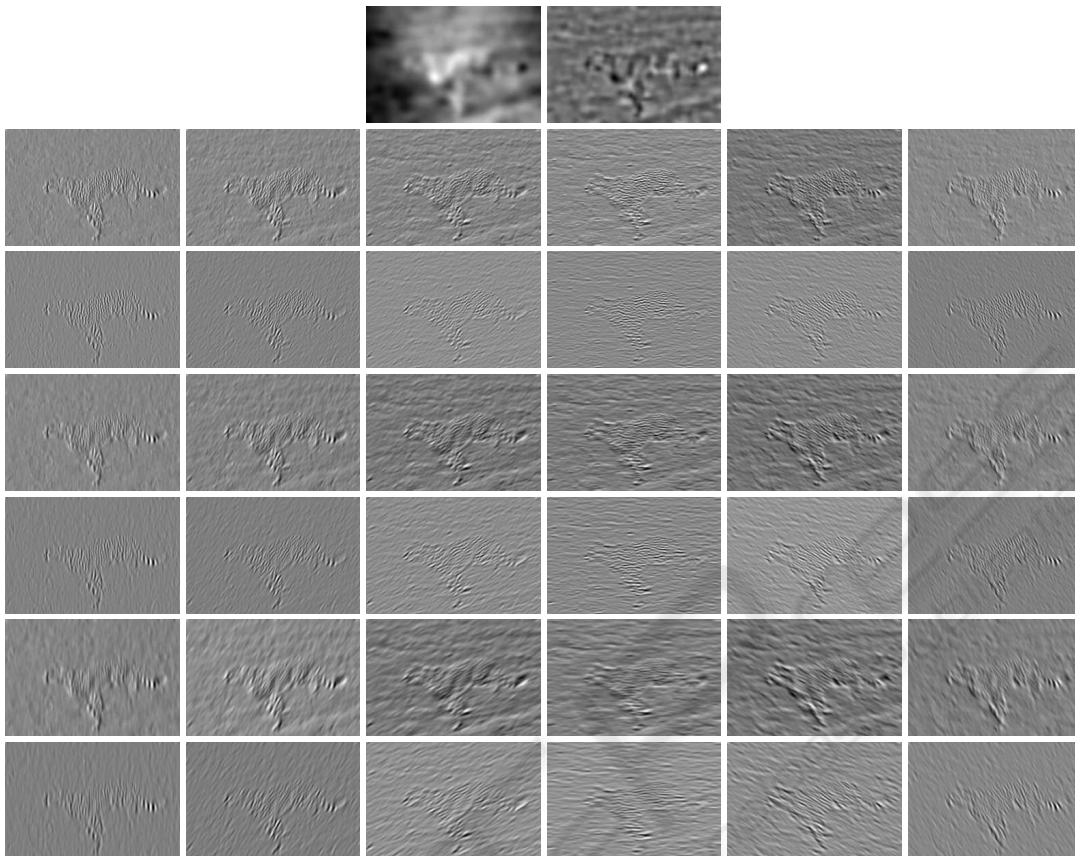


Figure 3: Filter responses.

spaced different orientations. This moderate size filter bank will produce a thirty eight dimensional feature space, which is considerably large for features extracted from a single image to populate. Fig. 3 gives the filter responses of the example image shown in Fig. 2. It is evidently clear that there are certain correlations among these filter responses and not all the channels are effectively revealing the image structures. Thus, it is natural to condense the feature space, which is particularly desirable for our application.

It is also worth noting that object in the scene may have inhomogeneous textures due to, for example, perspective projection. This inhomogeneity will exhibit nonuniform responses after applying directional filters, e.g. animal stripe texture (see zebra example in Fig. 7) and brick wall texture (see Fig. 8). Rotation invariance is thus desirable in such circumstance. We follow (Varma and Zisserman, 2002) to condense the filter responses by collecting only the maximum filter response across all the six orientations, i.e. those thirty six directional filter responses are reduced to six. Alternative methods, such as steerable filters (Jacob and Unser, 2004) can also be used. Thus, this not only reduces the dimensionality of the

feature space but also simultaneously achieves rotational invariance.

Instead of applying convolution operators, the recursive technique (Geusebroek et al., 2003) is used to efficiently filter the images. Fig. 4 shows the collected maximum responses from those thirty eight filter coefficients. Note the isotropic filter responses are remain unchanged since they are inherently rotationally invariant.

2.2 Local Spectral Histogram

The filtering responses can be directly used to drive the active contours as in, for example, (Sandberg et al., 2002). However, we can further incorporate local spatial dependency of filtering responses by computing the marginal distributions of filter responses over a local window. Thus, it captures local pixel dependency through filtering and global patterns through histograms. Local spectral histogram has been found useful, for example, texture classification (Liu and Wang, 2003). The maximum filter responses are largely local dominant features, such as edges and bars (e.g. see 4). Their spatial distribu-

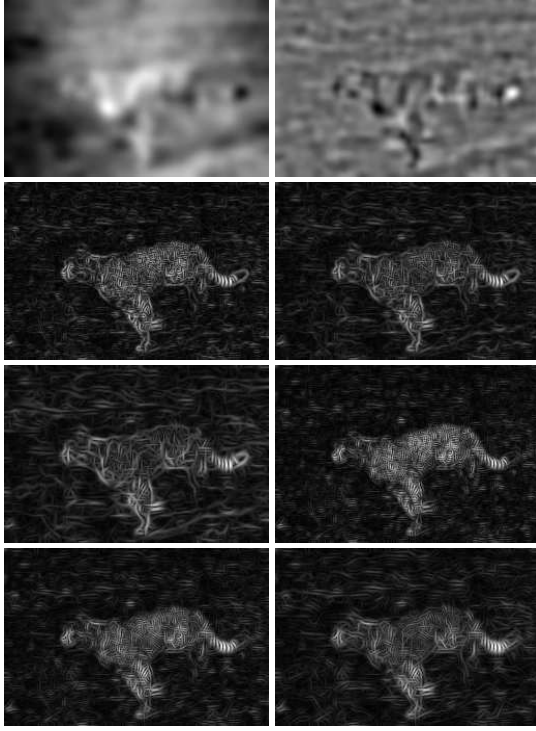


Figure 4: Maximum filter responses - The first row shows the filter responses from the isotropic Gaussian and Laplacian of Gaussian are kept the same. The rest six filter responses are collected from the 36 directional (isotropic) filter responses. Each of them contains the maximum responses across 6 different orientations (i.e. the six rows of the directional filter responses in Fig. 3 are collapsed into six rotational invariant filter responses).

tion conveys important information regarding the nature of the texture. Misaligning of filter responses due to inhomogeneity of filter responses can be a serious problem for direct approaches. Using local spectral histogram further enhances our model in dealing with texture inhomogeneity and helps to produce more coherent segmentation. Fig. 8 provides an example where directly using filter response and without taking into texture inhomogeneity resulted in a very poor segmentation, while as the proposed method correctly segmented the foreground object from the texturally nonuniform background.

Let \mathbf{W} denote a local window and $\mathbf{W}^{(\alpha)}(\mathbf{x})$ a maximum filter response patch centered at \mathbf{x} , where $\alpha = 1, 2, \dots, 8$. Thus, for $\mathbf{W}^{(\alpha)}$ the histogram is defined as (Liu and Wang, 2006):

$$P_{\mathbf{W}}^{(\alpha)}(z_1, z_2) = \sum_{\mathbf{x} \in \mathbf{W}} \int_{z_1}^{z_2} \delta(z - \mathbf{W}^{(\alpha)}(\mathbf{x})) dz, \quad (1)$$

where z_1 and z_2 specify the range of the bin. The spectral histogram is then defined as:

$$P_{\mathbf{W}} = \frac{1}{\mathbf{W}} \left(P_{\mathbf{W}}^{(1)}, P_{\mathbf{W}}^{(2)}, \dots, P_{\mathbf{W}}^{(8)} \right). \quad (2)$$

Example spectral histograms extracted from the testing image can be found in Fig. 6.

Very recently in (Ni et al., 2007), local image intensity histogram was used in the Chan-Vese model (Chan and Vese, 2001). However, this method may have difficulties in dealing with highly textured images where intensity alone is not sufficient to describe the texture. Intensity variation, for example, due to illumination changes can also cause severe problems. A comparative example is given in 9 where the best result reported in (Ni et al., 2007) is still significantly less accurate than the proposed approach.

2.3 Deducing Optimal Bin Size

Although histogram based methods have been routinely used in various image processing tasks, the importance of automatically selecting appropriate histogram bin size has been largely ignored. However, if a too small bin size is selected, the frequency value at each bin will suffer from significant large fluctuation due to the paucity of samples in each bin. On the other hand, if the bin size is chosen too large, the histogram will not be a good representation of the underlying distribution. Thus, it is necessary to select an optimal bin size. It also avoids the practical issues associated with manual parameter tuning.

We follow the method in (Shimazaki and Shinomoto, 2007) to estimate the optimal bin size. Let us consider a histogram as a bar graph. Also, let Δ denote the bin size. The expected frequency for $s \in [0, \Delta]$ is:

$$\theta = \frac{1}{\Delta} \int_0^{\Delta} \lambda_s ds, \quad (3)$$

where λ_s is the underlying true frequency which is not known. The goodness of fit of the estimated $\hat{\lambda}_s$ to λ_s is measured according to mean integrated squared error (MISE):

$$\text{MISE} = \frac{1}{\Delta} \int_0^{\Delta} \langle E(\hat{\theta} - \lambda_s)^2 \rangle ds, \quad (4)$$

where E denotes expectation and the empirical bar height $\hat{\theta}_i \equiv k_i/\Delta$ (k_i is the frequency count for i th bin). The associated cost function is then defined as:

$$o(\Delta) = \text{MISE} - \frac{1}{\Delta} \int_0^{\Delta} \langle (\lambda_s - \langle \theta \rangle)^2 \rangle ds. \quad (5)$$

The second term represents a mean squared fluctuation. By assuming the number of events counted in each bin obeys a Poisson distribution, the cost function can be written as:

$$o(\Delta) = \frac{2}{\Delta} \langle E\hat{\theta} \rangle - \langle E(\hat{\theta} - \langle E\hat{\theta} \rangle)^2 \rangle. \quad (6)$$

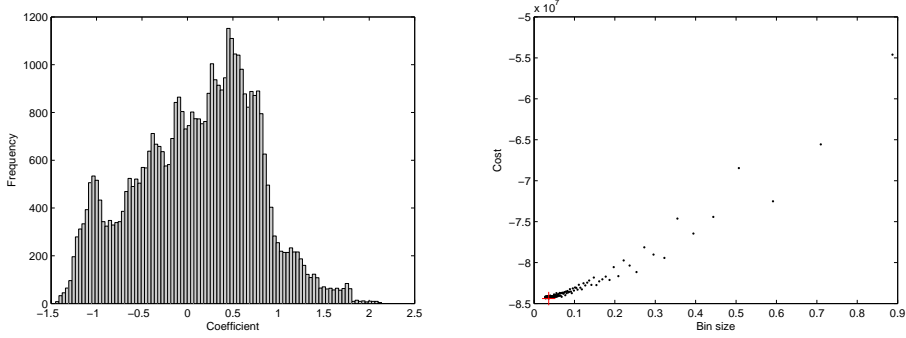


Figure 5: Optimal bin size selection - left: A typical spectral histogram for a single maximum response filter; right: The plot shows the relationship between the MISE based cost function and bin size (the red cross indicates the optimal bin size with the lowest MISE value).

The optimal bin size thus is obtained by minimizing the above cost function, i.e.

$$\hat{\Delta} = \arg \min_{\Delta} \mathcal{O}(\Delta). \quad (7)$$

Thus, the testing image is first filtered through the bank of isotropic and anisotropic filters and their responses are condensed into eight channels. Local spectral histograms at each pixel position are computed and histograms from the same channel are put together to produce a global histogram, i.e. mean local spectral histogram. Then, this optimal bin size selection is taken place for each of these eight mean local spectral histograms. Finally, all the local spectral histograms are finalized using the derived optimal bin size values. Fig. 5 gives an example of optimal bin size computation.

2.4 Active Contour based on Wasserstein Distance

The snake based segmentation can be viewed as a foreground-background partition problem (in the case of bi-phase). The snake evolves in the image domain, attempting to minimizing the feature similarity for those inside and outside the contours. Meanwhile, it tries to minimize the feature difference for those that are belong to the same region. Thus, we can formulate our snake based on the piece-wise constant assumption (Chan and Vese, 2001; Ni et al., 2007). However, since we are using invariant image features and local spectral histograms, the proposed method can cope with texture inhomogeneity much better than the original piece-wise constant model (see Figs. 8 and 9 as comparative examples).

Let Ω be the image domain, Λ_+ denote the regions inside the snake (foreground) and Λ_- those outside the snake (background). The snake segmentation

can be achieved by solving the following energy minimization problem:

$$\begin{aligned} \inf_{\Lambda_+} \mathcal{E}(\Lambda_+) = & \alpha \mathcal{L}(\Lambda_+) \\ & + \int_{\Lambda_+} \mathcal{D}(P(\mathbf{x}), P_+) d\mathbf{x} \\ & + \int_{\Lambda_-} \mathcal{D}(P(\mathbf{x}), P_-) d\mathbf{x}, \end{aligned} \quad (8)$$

where α is a constant, \mathcal{L} denote length, \mathcal{D} is the metric which measures the difference between two histograms, and P_+ and P_- are the foreground and background mean local spectral histograms to be determined. The first term is the length minimization term which regularize the contour. The next two terms are data fitting terms, which carry out the binary segmentation.

Among many other candidates, such as χ^2 distance and normalized cross correlation, The Wasserstein distance (also known as the earth mover's distance) (Rubner et al., 1998) is used to compute the distance between two normalized spectral histograms. since it is a true metric (unlike χ^2 distance) and has been found very useful in various applications, e.g. image retrieval (Rubner et al., 1998). Let $H_a(y)$ and $H_b(y)$ be two normalized spectral histograms. The Wasserstein distance between these two histograms is defined as:

$$\mathcal{D}(P_a, P_b) = \int_T |F_a(y) - F_b(y)| dy, \quad (9)$$

where T denoted the range of the histogram bins, and F_a and F_b are cumulative distributions of P_a and P_b , respectively.

The level set method is implemented to solve this energy minimization problem so that topological changes, such as merging and splitting, can be effectively handled. Let ϕ denote the level set function. The foreground is identified as $\Lambda_+ = \{\mathbf{x} \in \Omega : \phi(\mathbf{x}) >$

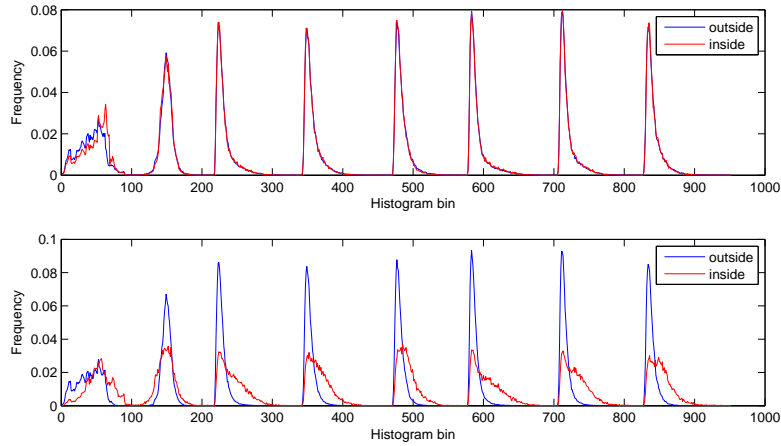


Figure 6: The average local spectral histogram inside and outside the snake - top: These two histograms are largely overlapping each other; bottom: It clearly shows the difference between the histograms when the snake converged to the object boundaries.

0}, which can be computed using the Heaviside function, i.e. $\int_{\Omega} \mathcal{H}(\phi) d\mathbf{x}$ where \mathcal{H} is the Heaviside function. The level set formulation can be expressed as:

$$\begin{aligned} \inf_{\Lambda_+} \mathcal{E}(\Lambda_+) = & \alpha \int_{\Omega} |\nabla \mathcal{H}(\phi)| d\mathbf{x} \\ & + \int_{\Omega} \mathcal{D}(P(\mathbf{x}), P_+) \mathcal{H}(\phi) d\mathbf{x} \quad (10) \\ & + \int_{\Omega} \mathcal{D}(P(\mathbf{x}), P_-) (1 - \mathcal{H}(\phi)) d\mathbf{x} \end{aligned}$$

The regularized Heaviside function proposed in (Chan and Vese, 2001) is used to allow larger support in the vicinity of the zero level set so that the contours can be initialized anywhere across the image (e.g. see Fig. 7):

$$\mathcal{H}_{\varepsilon}(z) = \frac{1}{2} \left(1 + \frac{2}{\pi} \arctan\left(\frac{z}{\varepsilon}\right) \right). \quad (11)$$

Thus, minimizing \mathcal{E} with respect to ϕ gives us the following partial differential equation:

$$\begin{aligned} \frac{\partial \phi}{\partial t} = & \delta_{\varepsilon}(\phi) \left[\alpha \nabla \cdot \left(\frac{\nabla \phi}{|\nabla \phi|} \right) \right. \\ & \left. - (\mathcal{D}(P(\mathbf{x}), P_+) - \mathcal{D}(P(\mathbf{x}), P_-)) \right] \\ = & \delta_{\varepsilon}(\phi) \left[\alpha \nabla \cdot \left(\frac{\nabla \phi}{|\nabla \phi|} \right) \right. \\ & \left. - \int_T |F_{\mathbf{x}}(y) - F_+(y)| dy \right. \\ & \left. + \int_T |F_{\mathbf{x}}(y) - F_-(y)| dy \right], \quad (12) \end{aligned}$$

where $\delta_{\varepsilon}(x) = \frac{d}{dx} \mathcal{H}_{\varepsilon}(x)$, F_+ and F_- are the spectral cumulative histogram inside and outside the contours, respectively. The minimization process thus moves

the contours towards object boundaries through competing pixels by measuring the similarity of local cumulative spectral histogram with those inside and outside current foreground.

Fig. 6 shows an example of spectral histogram changes between the initial stage and the stabilized result. The corresponding segmentation result can be found in the first row of Fig. 7.

3 RESULTS

The proposed method have been tested on both synthetic and real world images. Fig. 7 shows some typical examples results obtained using the proposed method. The first row shows the result of the running example given earlier. Good segmentation was achieved despite the large variations in the body region. In the second example, reasonable result was obtained, missing some very fine and thin structures. In the third example, there are clearly texture orientation variations. In the last two rows, the initial snakes were placed outside the objects of interest but still managed to localize them. Particularly, in the last example, there are significant texture variations both in foreground and background regions, which made it very difficult to segment.

In Figs. 8 and 9, we mainly compare our work with two extensions of the piece-wise constant model, which is also our fundamental model. Fig. 8 demonstrates when dealing with inhomogeneous textures, the proposed method performs significantly better than that directly using filter responses (Sandberg et al., 2002). The proposed method also showed improvements against a very recent method based on lo-

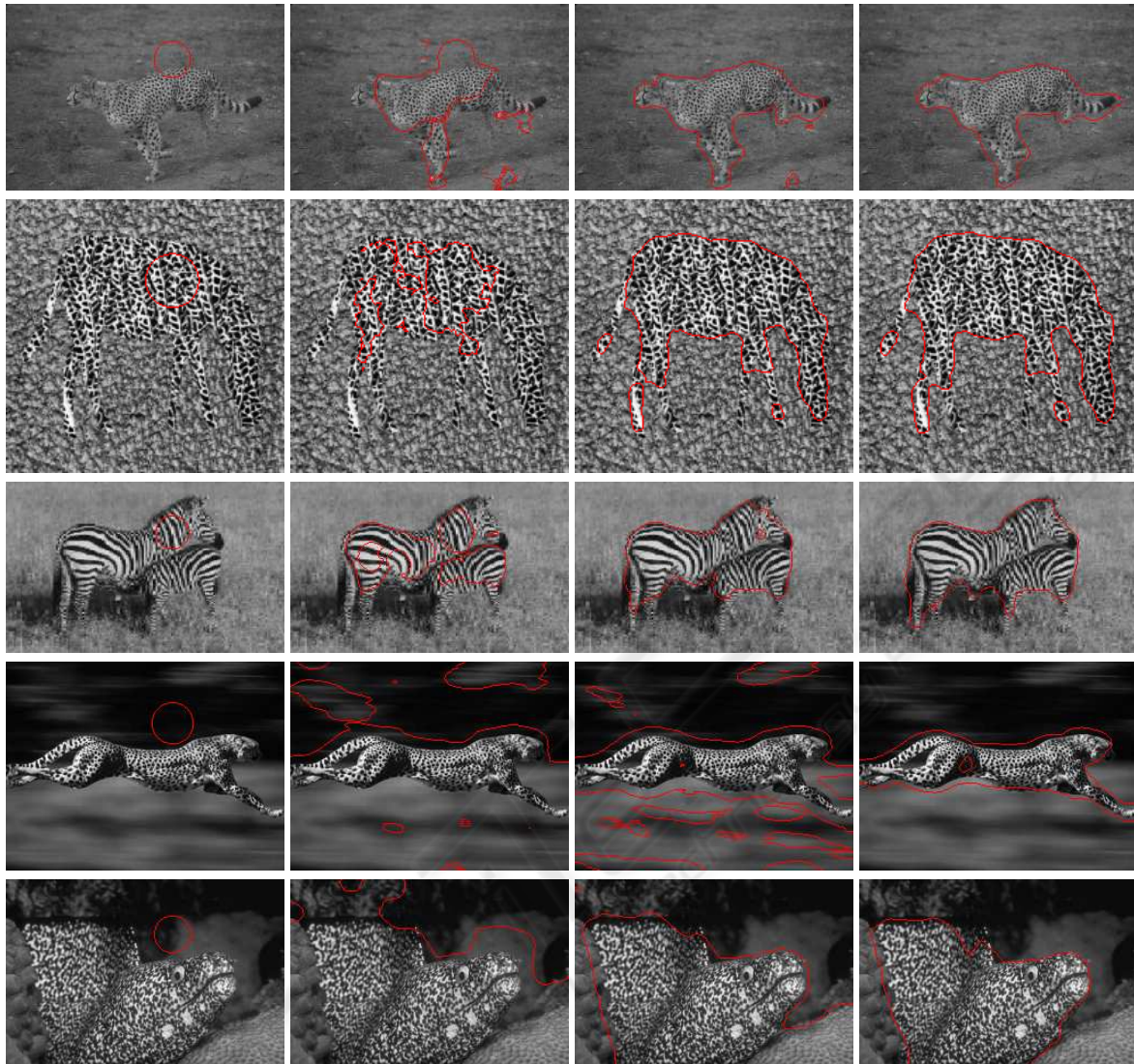


Figure 7: Examples results of the proposed method - from left: initial snake, intermediate stages, and stabilized results.

cal histograms (Ni et al., 2007). It illustrates the effectiveness of using invariant filtering technique. Fig. 9 also gives example results obtained from geodesic snake and generalized GVF snake (Xu and Prince, 1998). It is expected that these edge based techniques are not appropriate when dealing with highly textured images.

The proposed method requires very little parameter tuning. All the images given in this paper are using a fixed set of parameters. The parameters used to generate the filter bank are given in Section 2.1. The local window used to collect the spectral histogram is empirically fixed as 19. For a too small window size, the local spectral histogram may have difficulties in reflecting underlying distribution and can result in isolated regions. For a too large window, the segmen-

tation can be less accurate around object boundaries. We found that a window size of 19 is a good trade-off, however, we attempt to automatically select the window size as part of our future work. The parameter α controls the smoothness of the contour and very rarely needs adjustment. As for computational complexity, the proposed method is very similar to (Sandberg et al., 2002).

4 CONCLUSIONS

In this paper, we introduced a novel region based snake method which is based on the assumption that foreground and background local filtering response distributions are statistically separable. Maximum re-

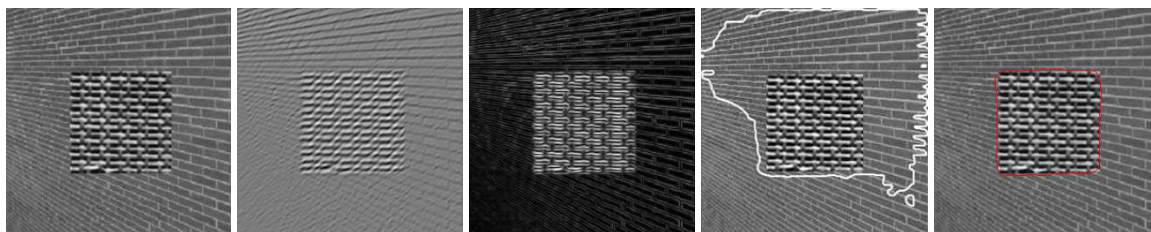


Figure 8: From left: a synthetic texture collage which contains an inhomogeneous background due to orientation and scale changes; a filter response to a particular orientation; the maximum response derived across different orientations which highlights edge features in various directions, including vertical; segmentation result obtained using the Chan-Vese model based on Gabor features (Sandberg et al., 2002) (result reported in (Sagiv et al., 2006)); segmentation result obtained using the proposed method.



Figure 9: Comparative analysis - first two images: results obtained using edges based methods, namely geodesic snake and generalized GVF snake (Xu and Prince, 1998); third image: best result on the testing image reported in (Ni et al., 2007) using a region based approach; last image: result obtained using the proposed method.

sponses filters were used to achieve rotational invariance and their local spectral histograms were used as image features to drive the snake. The experimental studies showed some very promising results. As part of our future work, we will further investigate optimal filter selection and automatic local spectral histogram window selection.

ACKNOWLEDGEMENTS

The recursive filtering is based on the library provided by (Geusebroek et al., 2003).

REFERENCES

- Aujol, J., Aubert, G., and Blanc-Féraud, L. (2003). Wavelet-based level set evolution for classification of textured images. *IEEE T-IP*, 12(12):1634–1641.
- Chan, T. and Vese, L. (2001). Active contours without edges. *IEEE T-IP*, 10(2):266–277.
- Geusebroek, J., Smeulders, A., and van de Weijer, J. (2003). Fast anisotropic gauss filtering. *IEEE T-IP*, 12(8):938–943.
- He, Y., Luo, Y., and Hu, D. (2004). Unsupervised texture segmentation via applying geodesic active regions to Gaborian feature space. *IEEE Trans. Eng. Comput. Technol.*, pages 272–275.
- Houhou, N. and Thiran, J. (2008). Fast texture segmentation model based on the shape operator and active contour. In *IEEE CVPR*, pages 1–8.
- Jacob, M. and Unser, M. (2004). Design of steerable filters for feature detection using Canny-like criteria. *IEEE T-PAMI*, 26(8):1007–1019.
- Liu, X. and Wang, D. (2003). Texture classification using spectral histograms. *IEEE T-IP*, 12(6):661–670.
- Liu, X. and Wang, D. (2006). Image and texture segmentation using local spectral histograms. *IEEE T-IP*, 15(10):3066–3077.
- Ni, K., Bresson, X., Chan, T., and Esedoglu, S. (2007). Local histogram based segmentation using the Wasserstein distance. In *Scale Space and Variational Methods in Computer Vision*, pages 697–708.
- Paragios, N. and Deriche, R. (2002). Geodesic active regions and level set methods for supervised texture segmentation. *IJCV*, 46(3):223–247.
- Paragios, N., Mellina-Gottardo, O., and Ramesh, V. (2004). Gradient vector flow geometric active contours. *IEEE T-PAMI*, 26(3):402–407.
- Pujol, O. and Radeva, P. (2004). Texture segmentation by statistical deformable models. *International Journal of Image and Graphics*, 4(3):433–452.
- Rousson, M., Brox, T., and Deriche, R. (2004). Active unsupervised texture segmentation on a diffusion based feature space. In *IEEE CVPR*, pages 1–8.
- Rubner, Y., Tomasi, C., and Guibas, L. (1998). A metric for distributions with applications to image databases. In *IEEE CVPR*, pages 59–66.
- Sagiv, C., Sochen, N., and Zeevi, I. (2006). Integrated active contours for texture segmentation. *IEEE T-IP*, 15(6):1633–1645.
- Sandberg, B., Chan, T., and Vese, L. (2002). A level-set and gabor-based active contour algorithm for segmenting

- textured images. Technical Report 39, Math. Department UCLA, Los Angeles, USA.
- Savelonas, M., Iakovidis, D., and Maroulis, D. (2008). LBP-guided active contours. *Pattern Recognition Letters*, 29(9):1404–1415.
- Shimazaki, H. and Shinomoto, S. (2007). A method for selecting the bin size of a time histogram. *Neural Computation*, 19(6):1503–1527.
- Varma, M. and Zisserman, A. (2002). Classifying images of materials: Achieving viewpoint and illumination independence. In *ECCV*, pages 255–271.
- Xie, X. and Mirmehdi, M. (2008). MAC: Magnetostatic active contour model. *IEEE T-PAMI*, 30(4):632–646.
- Xu, C. and Prince, J. (1998). Snakes, shapes, & gradient vector flow. *IEEE T-IP*, 7(3):359–369.

